PNAS Nexus, 2024, 3, pgae341
https://doi.org/10.1093/pnasnexus/pgae341
Advance access publication 21 August 2024
Research Report

Bio-molecular analyses enable new insights into the taphonomy of feathers

Yanhong Pan [a,*], Zeming Qi [b], Jianfang Hu [c], Xiaoting Zheng [d,e] and Xiaoli Wang [d,e]

[a]State Key Laboratory for Mineral Deposits Research, School of Earth Sciences and Engineering, Centre for Research and Education on Biological Evolution and Environment, Frontiers Science Center for Critical Earth Material Cycling, Nanjing University, Nanjing 210023, China
[b]National Synchrotron Radiation Laboratory, University of Science and Technology of China, Hefei 230027, China
[c]State Key Laboratory of Organic Geochemistry, Guangzhou Institute of Geochemistry, Chinese Academy of Sciences, Guangzhou 510640, China
[d]Institute of Geology and Paleontology, Linyi University, Linyi City, Shandong 276005, China
[e]Shandong Tianyu Museum of Nature, Pingyi, Shandong 273300, China
*To whom correspondence should be addressed: Email: panyanhong@nju.edu.cn
Edited By Zhonghe Zhou

Abstract

Exceptionally preserved feathers from the Mesozoic era have provided valuable insights into the early evolution of feathers and enabled color reconstruction of extinct dinosaurs, including early birds. Mounting chemical evidence for the two key components of feathers—keratins and melanins—in fossil feathers has demonstrated that exceptional preservation can be traced down to the molecular level. However, the chemical changes that keratin and eumelanin undergo during fossilization are still not fully understood, introducing uncertainty in the identification of these two molecules in fossil feathers. To address this issue, we need to examine their taphonomic process. In this study, we analyzed the structural and chemical composition of fossil feathers from the Jehol Biota and compared them with the structural and chemical changes observed in modern feathers during the process of biodegradation and thermal degradation, as well as the structural and chemical characteristics of a Cenozoic fossil feather. Our results suggest that the taphonomic process of feathers from the Cretaceous Jehol Biota is mainly controlled by the process of thermal degradation. The Cretaceous fossil feathers studied exhibited minimal keratin preservation but retained strong melanin signals, attributed to melanin's higher thermal stability. Low-maturity carbonaceous fossils can indeed preserve biosignals, especially signals from molecules with high resistance to thermal degradation. These findings provide clues about the preservation potential of keratin and melanin, and serve as a reference for searching for those two biomolecules in different geological periods and environments.

Significance Statement

The preservation of organic molecules in fossils has opened a unique window into investigating the molecular evolution of extinct organisms in deep time. However, to characterize chemically the organic molecules retained in fossils is challenging, because the organic molecules preserved in fossils have undergone more or less diagenetic modifications, which necessitates the application of multiple independent techniques and investigations of the taphonomic pathways. In this work, we suggest that dehydration played a role in the exceptional preservation, and low-maturity carbonaceous fossils can indeed preserve biosignals, especially signals from molecules with high resistance to thermal degradation. Our findings should be of great interest to paleontologists, evolutionary biologists, and the general public.

Introduction

Fossil feathers are crucial for understanding the early evolution of feathers, flight, and the biology of dinosaurs, including early birds (1–3). Despite recent progress (4–8), the chemical nature of fossil feathers remains incompletely understood. The structural proteins of modern feathers are primarily composed of β-keratins (also known as corneous beta-proteins) with small amounts of α-keratins (9). The protein composition significantly affects the physical and mechanical properties of feathers (10, 11). Immunological studies have suggested that early feathers may have been dominated by α-keratins rather than by β-keratins (7). However, some researchers argued that the immunological methods are prone to false positives (12–14).

In addition to keratins, many dark-colored feathers contain melanins, including brown to black eumelanins and yellow to reddish pheomelanins, which are stored in melanosomes (15). Chemical evidence of melanins—mainly eumelanins, as pheomelanin markers are difficult to resolve in fossils (16)—supports the identification of melanosomes in fossils (4, 5). The morphology of these melanosomes has been useful in reconstructing the

Competing Interest: The authors declare no competing interest.
Received: June 7, 2024. **Accepted:** July 29, 2024

colors of extinct animals (17–20). However, it remains unexplored whether various degraded forms of eumelanins can be distinguished in fossils, which is essential for understanding the chemical and functional evolution of eumelanins.

In this study, we employed time-of-flight secondary ion mass spectrometry (Tof-SIMS), Fourier transform infrared spectroscopy-attenuated total reflection (FTIR-ATR), and Raman spectroscopy to characterize the protein and melanin remains in both fossil and modern feathers. Our aim was to trace the chemical changes that keratin and eumelanin undergo during fossilization, and to distinguish the degraded products from keratins and eumelanins in fossil feathers from as early as the Early Cretaceous. We analyzed fossil feathers from four specimens: three from the Early Cretaceous Jehol Biota of northeastern China, housed at the Shandong Tianyu Museum of Nature (STM) (including two enantiornithine birds STM7-26 and STM7-27, and one early ornithuromorph bird STM8-23), and one isolated feather from the Oligocene of the Tibetan Plateau (referred to as TF) (Fig. S1).

Results

Scanning electron microscopy observations

Under scanning electron microscopy (SEM), cracks were observed in all the fossil feathers, indicative of dehydration (Fig. 1A, C, F, I). Higher magnification SEM images revealed melanosomes and surrounding matrices that are likely residues of the originally keratinous matrices in the Early Cretaceous feathers STM7-26 (Fig. 1B), STM7-27 (Fig. 1D and E), and STM8-23 (Fig. 1G). A comparison of the length and diameter of the melanosomes showed that the melanosomes in the three samples differ in geometry (Fig. 1L). The mean aspect ratio was 5.00 for STM7-26, 6.35 for STM7-27, and 2.83 for STM8-23. Unlike the Cretaceous samples, the Oligocene feather sample (TF) appears to be contaminated by recent microbes (Fig. 1J), based on the following observations: these microbes are lying on the surface, deformed in line with the topography of the surface; they are excavated by multiple pit-shaped fossae; and similar microbodies—though showing weaker holes—are observed in the host sediment matrix (Fig. 1K), consistent with microbial death and subsequent biodegradation.

Tof-SIMS analysis

We used a chicken feather and melanin from the common cuttlefish (*Sepia officinalis*) as references. Tof-SIMS showed peaks characteristic of amino acids (Fig. S2, Table S1) (21–23) in the positive ion spectra of all fossil feathers and associated sediments, as well as the melanin reference. Principal component analysis (PCA) was employed to identify variations among the samples. PCA results showed that the Early Cretaceous feathers STM7-26 and STM7-27 are well separated from their sediments associated with STM7-26 and STM7-27 along PC2 (Fig. 2A), and together with feather STM8-23, they fall between the keratin reference and the melanin reference along PC1 (Fig. 2A). We noted that the melanin reference also contains proteins (Fig. S2), consistent with previous studies (24).

Negative-ion Tof-SIMS spectra from all samples showed features characteristic of eumelanin (5), except for the modern chicken feather reference (Fig. S3). PCA was also employed to identify variations among the samples (Fig. 2B). Results showed that all three Early Cretaceous feathers fall close to the melanin reference, but separate from the associated sediments in the chemospace (Fig. 2B). Since eumelanin was concentrated within melanosomes, which are covered and mixed with keratins in modern chicken feathers, Tof-SIMS failed to record the negative characteristic peaks of eumelanins.

However, PCA results on both the 9 positive characteristic peaks of amino acids and 38 negative ions characteristic peaks of eumelanins showed that the Oligocene feather (TF) falls close to its associated sediment. Tof-SIMS detects signals from the top molecular layer of the sample, so the characteristic Tof-SIMS peaks are from the microbes covering the surface of the TF sample as well as the associated sediment.

These results suggest that Tof-SIMS is so sensitive to organic fragments that it is usually unable to identify either endogeneous protein or melanin remains from the occurrence of "melanin-characteristic" or "protein-characteristic" ions alone. When PCA analysis was employed, our results indicate that both the positive and negative ions of Tof-SIMS signals from the Early Cretaceous feathers are well separated from the associated sediments.

ATR-FTIR analysis

The ATR-FTIR spectra of the Cretaceous feathers (STM7-26, 7-27, 8-23) have a broad band at the region of 1,580 – 1,560 cm^{-1} (Fig. 3A and B), which is assignable to C=C stretching of indole and pyrrole rings. Both the spectra of the melanin and humid acid references showed a similar broad band at the same region (1,568 cm^{-1} in Fig. 3A and B). Besides, the ATR-FTIR spectra of STM7-27, STM8-23, TF and their associated sediments all have a strong band at ~1,420 cm^{-1}, which is due to CO_3^{2-} (25). However, the spectrum of STM7-26 has a band at 1,374 cm^{-1} instead of 1,420 cm^{-1}, and its associated sediments do not have an observable band at 1,420 cm^{-1} either. The band at 1,374 cm^{-1} of STM7-26 can be due to C–N stretching combined with in-plane deformation of O–H and ring stretching (24). The large broad band centered at ~3,300 cm^{-1} assigned to O–H stretching (O–H and/or N–H). The band at ~2,927 cm^{-1} (asymmetric C–H of aliphatic CH_3), and 2,854 cm^{-1} (asymmetric and symmetric C–H of aliphatic CH_2) could be assigned to C–H stretching. The spectrum of the Oligocene feather (TF) has two shoulder bands at around 1,640 cm^{-1} and 1,540 cm^{-1}, which are assignable to C=O of Amide I and C–N and N–H of Amide II. However, its associated sediment has these two shoulder bands too, although a bit weaker, which seems to be consistent with the presence of microbes on the surface of the sample.

The Synchrotron (SR) enhanced ATR-FTIR spectra of the fossil feathers are almost coincidence with the ATR-FTIR spectra. All Cretaceous feathers (STM7-26, 7-27, 8-23) have a broad band at the region of 1,575 – 1,545 cm^{-1} (Fig. 3A and B); STM7-27, STM8-23, TF and their associated sediments all have a strong band at 1,418 cm^{-1}, but STM7-26 has a band at 1,380 cm^{-1}. However, the SR-ATR-FTIR spectra presented more details in the region of 1,200 – 1,800cm^{-1}. For example, instead of two shoulder bands at around 1,640 and 1,540 cm^{-1} of the ATR-FTIR spectrum, the SR-ATR-FTIR of TF showed a strong bands at 1,553 cm^{-1} with a shoulder band at 1,641 cm^{-1}. STM7-27, STM8-23, TF shows two shoulder bands of at ~1,450 and ~1,376 cm^{-1}.

PCA analysis was employed on the 1,720 – 1,480 cm^{-1} region of the spectra of the fossil feathers, the extant chicken feather, melanin from *S. officinalis*, humic acid, and the samples from maturation experiments (Fig. 3C and D). PCA result showed that the fossil feathers, eumelanin and humic acid references are separate from untreated and experimentally matured chicken feathers (details see Fig. S6) along PC1 (Fig. 3C). According to the loadings, PC1 explained the variations of the relative abundance of Amide I and II vs. components containing indole and pyrrole rings (Fig. 3D). The Early Cretaceous fossil feathers were located

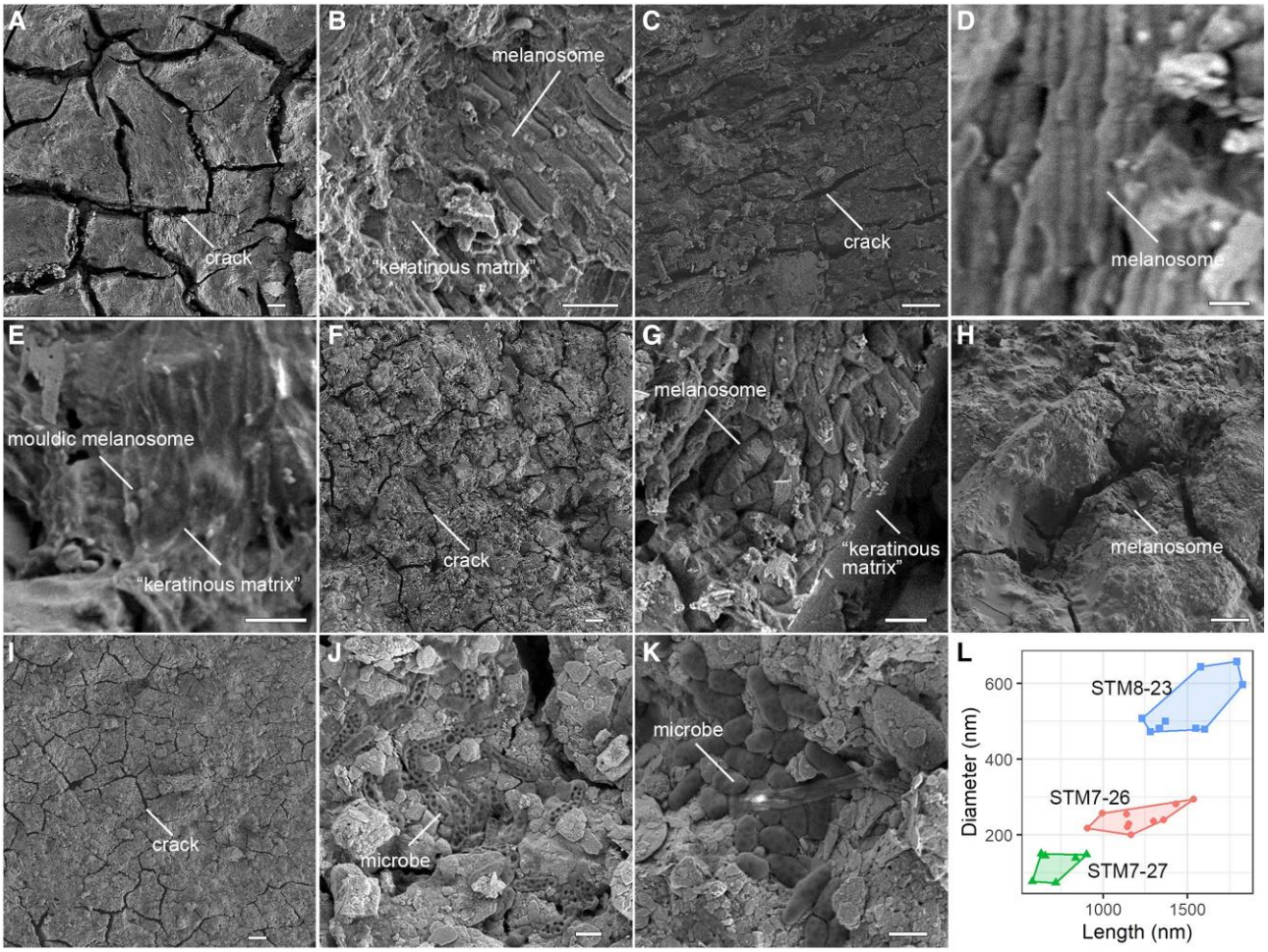

Fig. 1. Microstructures of fossil feathers from the Early Cretaceous and the Oligocene. A,B) STM7-26. C–E) STM7-27. F–H) STM8-23. I–L), Isolated Oligocene feather (I, J) and associated sediment (K). L) Comparison of the melanosomes in the three Early Cretaceous feather samples. Scales bars, 10 μm (A, C, F, H, I); 1 μm (B, G, J, K); 200 nm (D); 500 nm (E).

between the eumelanin and humic acid, while TF feathers were located between the eumelanin and the untreated and experimentally matured chicken feathers. The highly matured chicken feather samples (A4 in Fig. 3C) are separate from the untreated and moderated matured chicken feathers along PC1, which reflects their lower abundance of Amide I and II (Fig. 3D). According to the loadings of PC2, higher scores indicate higher abundance of β-turn or quinone C=O, and higher content of components contains indole and pyrrole rings. The highly matured chicken feathers (A4 in Fig. 3C) separated from the other chicken feathers (untreated and moderately matured) along PC2.

Raman spectroscopy analysis

The Raman spectra of all fossil feathers have two broad bands at 1,353 – 1,360 and 1,587 – 1,591 cm^{-1} (Fig. 4A), similar to previously reported spectra of eumelanins in feathers of extant birds (26) and our eumelanin reference (Fig. 4A). As previously noted for the disordered graphite of carbonaceous materials from geological sediments (27, 28), which displayed the Raman spectra pattern with two similar bands, carbonaceous materials in sediments from the Yixian Formation and humic acid used as controls in this study yield Raman bands with similar wavenumbers as the fossil feathers (Fig. 4A).

However, the shape of the two bands is different, so we performed PCA analysis to compare these spectra. Principal component 1 explained 73.6% of the total variation. Our analysis revealed that carbonaceous materials (structureless organic remains) in sediments (Fig. S7) and humic acids are distinct from melanin references along PC1. The melanin references included nature melanin from the common cuttlefish (*S. officinalis*, Sigma-Aldrich M2649) and melanin signals from modern feathers (a mixture of eumelanin and pheomelanin). Fossil feathers fall between them (Fig. 4B). The three bands loading positively into PC1 at 1,268, 1,368, and 1,605 cm^{-1} can be assigned to three of the five detail deconvoluted peaks in the first-order Raman spectra of disordered graphite, specifically D4, D1, and D2, respectively (27) (Fig. 4C). The band loading negatively into PC1 at 1,527 cm^{-1} can be assigned to pyrrole, which is characteristical function group of eumelanins (29).

Discussions

Contamination issues

Contamination is a common problem in molecular palaeontolgy (30, 31), partly because the porosity of sediments allows exogeneous amino acids and other biomolecules to enter the fossils (32, 33). Thus, signals from the associated sediment are always compared with those from the fossils. By sampling the surrounding sediments, we can establish a baseline for the organic compound present in the environment. This allows us to compare the organic

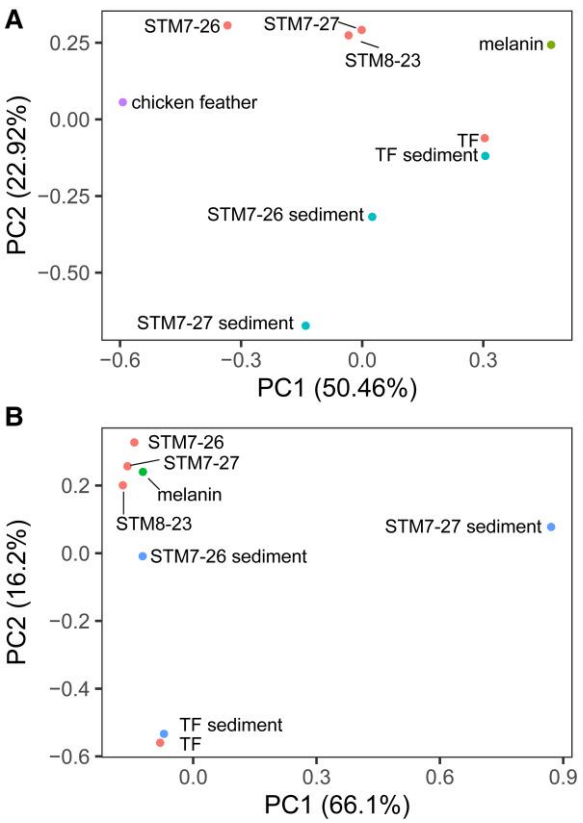

Fig. 2. PCA comparing ToF-SIMS spectra from fossil feathers with sediments and modern references. A) PCA of positive ions characteristic of amino acids in positive ion ToF-SIMS spectra. B) PCA of negative ions characteristic of melanins in negative-ion ToF-SIMS spectra. See Fig. S4 for loadings for the first two PCs in (A), and Fig. S5 for loadings for the first two PC2 in (B).

composition of the feather with that of the sediments. If the organic signals from the feather match those found in the sediments, it suggests potential contamination. Conversely, if the feather's organic composition is distinct from the sediment, it supports the hypothesis that the organic material is endogenous. In our work, FTIR-ATR detected Amide I and Amide II signals from both the Oligocene TF feather and its associated sediment. Tof-SIMS detected protein-related ions from both the Oligocene TF feather and its associated sediment, with almost the same intensities. Furthermore, our SEM observations documented microbes growing on the surface of the TF feather and its associated sediment. Similarly, Manning et al. (31) found amino acids from both the skin of a well-preserved dinosaur and the associated sediment. Therefore, it is crucial to determine the endogeneity of the chemical signals when analyzing fossil samples (8). Our PCA analysis of the Tof-SIMS data and ATR-FTIR and SR-ATR-FTIR spectra all indicate that the Cretaceous feathers differ from the sediment in organic composition, suggesting that the organic signals from these samples should be more likely endogenous.

Preservation of keratins in fossils

Tof-SIMS showed peaks characteristic of amino acids from all the Cretaceous feathers, and PCA analysis separated them from their associated sediments. However, except for the TF feather, the FTIR spectra from all Cretaceous fossil feathers do not show any appreciable bands at ~1,630, ~1,518, and ~1,235 cm^{-1} assigning to amide I, amide II, and amide III, respectively, as seen in extant feather, indicating an almost complete protein loss, or at least the content under the detection limit of the instrument.

All fossil feathers display a similar SR- ATR-FTIR spectrum in the range of 1,200–1,800 cm^{-1}. We detected a strong and broad band at ~1,545 – ~1,575 cm^{-1} and two relatively weak bands at ~1,450 and ~1,375 – ~1,380 cm^{-1} on all fossil feathers, including the TF feather. The band at ~1,545 – ~1,575 cm^{-1} is assignable to C=C stretching of indole and pyrrole rings, which is common in either melanin or humic acid (34, 35). Another characteristic band of melanin is at ~1,347 – 1,321 cm^{-1}, which is absent in the FTIR spectra from all fossils. All the fossil feathers have a band at ~1,375 – ~1,380 cm^{-1} assignable to C–N stretching combined with in-plane deformation of OH and ring stretching (29), which is comparable to the band at 1,371 cm^{-1} of the humic acid. However, almost all fossil feathers have a shoulder band at ~1,450 cm^{-1}, which is absent in the reference spectrum from humic acid.

FTIR spectra from fossil feathers have also been reported in previous studies (36, 37). Both works recorded a strong band at ~1,600 – 1,560 cm^{-1}, which was attributed to carboxylate, and a broad band at ~1,450cm^{-1} – ~1,330 cm^{-1}, with different interpretations, either related to the presence of $CaCO_3$ (37) or referred to carboxylic acid and hydroxyl from the melanin (36). When we looked at the SEM images from the previous two works, there is no clear evidence that the fossil feathers contained a carbonaceous matrix enveloping the melanosomes (36, 37). According to our results, the infrared (IR) spectra pattern showed more similarities to the humic acid reference than the melanin reference. Nevertheless, proteinaceous components that might be from keratins have been detected in several fossils by FTIR spectra (e.g. (31, 38, 39)). Amide I and II bands were detected in a mummified skin from an Upper Cretaceous hadrosaur dinosaur (31). Amide I, II, and III absorption bands, along with the C–H peaks, were present in the full spectrum from an Eocene aged fossil reptile skin, and FTIR mapping further supported the endogenous origin of the proteinaceous components within the fossilized soft tissue (38). The oldest record is from carbonaceous filaments of a mid-Late Jurassic pterosaur, with the presence of the amide I and II bands in the FTIR record (39), which is much older than our Cretaceous feathers. Their studied materials show weaker melanin signals than the fossil feathers in this study, which contain abundant melanosomes. This discrepancy suggests two possible explanations: (i) our fossil feathers may have displayed extremely weak signals of these amide peaks, which were subsequently overshadowed by the strong melanin signals; and (ii) the keratins in the fossil feathers may have undergone significant alteration, transforming into thermally stable organic compounds.

Implications for the fossilization process of keratins in feathers

Detecting biomolecules in ancient fossil is challenging because organic molecules of biological origin are inevitably altered and degraded during fossilization. When organisms die their organic molecules usually rapidly biodegrade. Most biomolecules released into the environment are either oxidized or assimilated by living microbes. Yet, some organic macromolecules resistant to biodegradation may escape and be incorporated into fossils by selective preservation. Modern feathers contain 80–90% keratin (the main structural protein of feather). Keratins contain a high percentage of stable beta-pleated sheets (beta-sheet, more than 70%), and amino acids are cross-linked via covalent disulfide and hydrogen bonds, resulting in low solubility and high stability (40–42). Such complex, rigid, and fibrous features make keratin highly resistant

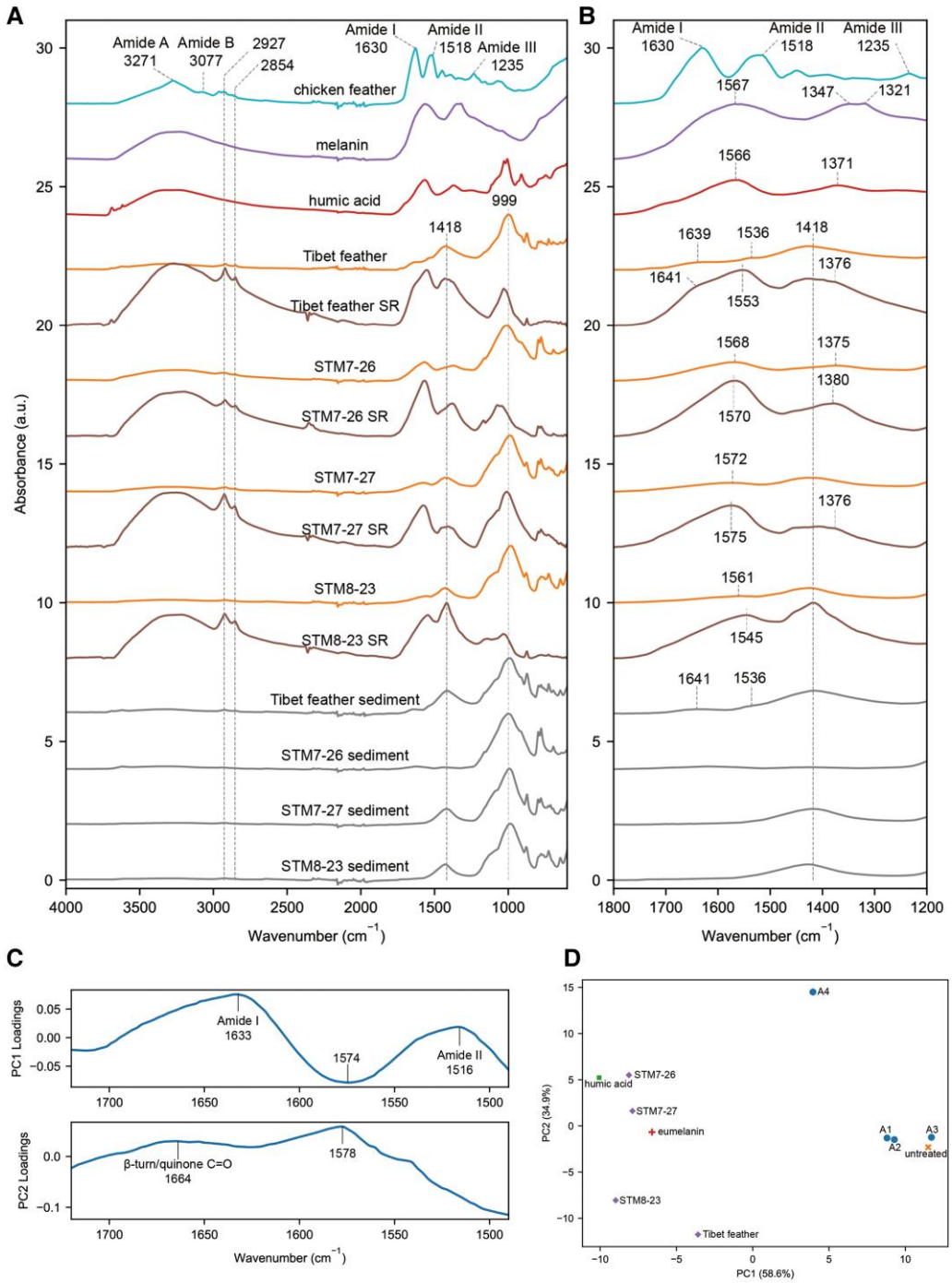

Fig. 3. ATR-FTIR analysis of fossil feathers and comparative samples. A) FTIR spectra of fossil feathers and surrounding sediments, modern feather, melanin from the common cuttlefish (*S. officinalis*), and humic acid. B) Details of ranges between the 1,200 and 1,800cm^{-1} of whole spectra. C) Loadings for the first two PCs from PCA. D) Score plot from PCA of whole spectra.

and unable to be easily biodigested by common proteases except keratinase (42, 43). Despite the high resistance, keratins do not accumulate in nature, which indicates the presence of natural biodegradation (44). Keratinases are ubiquitous in nature and can be found in bacteria and fungi (45–47). With the help of keratinase, bacteria or fungi are capable of decomposing keratin, and the process involves two steps: sulfitolysis and proteolysis (48–50). Sulfitolysis refers to the cleavage of disulfide bonds, which will change the conformation of keratins and provide more sites for keratinase (46, 51, 52). The biodegradation of feathers by bacteria and fungi has been systematically studied for decades, and the breakdown of feather microstructure has been visualized using SEM with various bacteria and fungi (51, 53–57). The course of degradation exhibits a similar pattern: degradation appeared as breakage of the barbules, exposure of the internal fiber structure; then the degradation of feather barbs; and finally, the rachis structure (or the feather shaft). However, as seen, the fossil feather is intact with all shafts and vanes in place, and the integrity of the barbs was maintained (Fig. S1), indicating that the biodegradation seems inhibited. Nevertheless, it is important to note that keratinolytic enzymes are mainly inducible (46, 58, 59). The production of keratinase is usually associated with the adaption to stationary

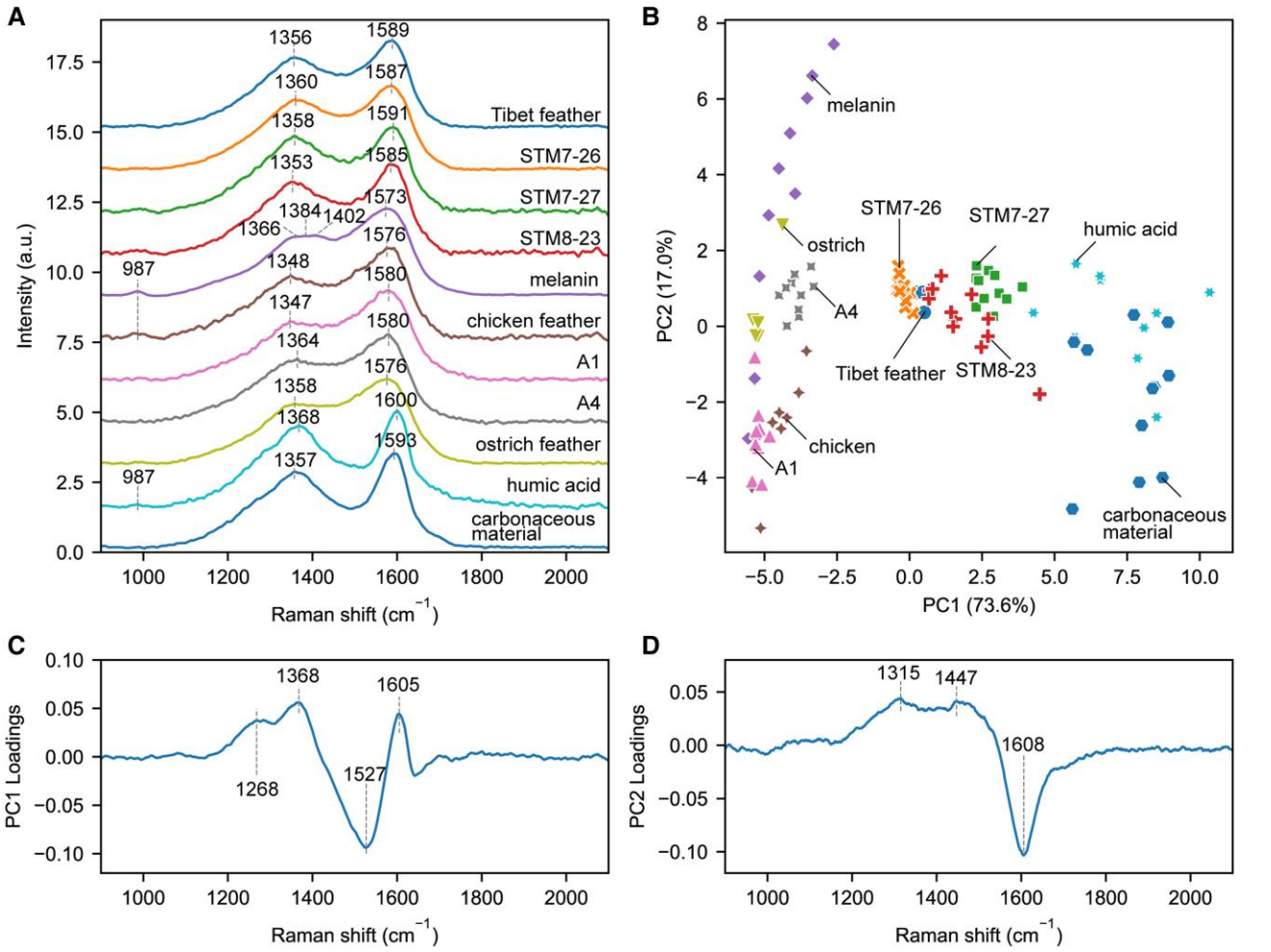

Fig. 4. Comparison of different melanins and carbonaceous materials using Raman microscopy. A) Raman spectra of fossil feathers, modern feathers, melanin from the common cuttlefish (*S. officinalis*), and carbonaceous materials in sediments from the Yixian Formation. B) Score plot from PCA of whole spectra. C, D) Loadings for the first two PCs from PCA. A1, A4 in Panel A refer to samples matured in an open system with water at temperature settings 1 and 4, respectively (see Supplementary information for details).

phase or lack of nutrients (60, 61). In the case of the Jehol Biota, the palaeolake is most likely rich in nutrients (62, 63). Furthermore, most research recorded neutral or alkaline pH (7.0–10.0) and high temperature (30–80°C) as the optimal condition for bacterial keratinase (46, 64–71). The dissolution of the shell carbonate of the occasionally occurring bivalves collected from the finely laminated sediments of the Yixian Formation (72, 73) and phosphatized claw sheaths, carapaces, and eggs of the clam shrimps from the Jehol Biota (74, 75) indicated a slightly acidic environment at the bottom of the palaeolake. All of these are reasons that might hindered the biodegradation of keratins or made the feathers of the Jehol Biota more resistant to biodegradation during the fossilization process.

As preserved in carbonaceous compressions, besides the biodegradation process, fossil feathers should have been subjected to a long-term thermal maturation. Our FTIR spectra reveal a close similarity between the preserved organic functional groups present in the fossils and the humic acid, implying the effect of the long-term thermal maturation process. With increasing temperature, weaker organic bonds are thermally broken, and dehydrogenation reactions become predominant. Thermal maturation may ultimately lead to pure graphite that may have completely lost its original biosignatures by promoting structural reorganization (76). In most cases, the IR spectrum recorded from the organic composition of fossil remains showed contributions from both aliphatic and aromatic functional groups (76, 77), which is characterized by the CH_3 and CH_2 absorptions at 3,000 – 2,800 cm^{-1} spectral interval and the combined bending vibrations of CH_3 and CH_2 at 1,500 – 1,300 cm^{-1} spectral region. Such diagenetically transformed products could be from a variety of original biomolecular makeups. Sometimes, besides diagenetic hydrocarbons, traces of the original biomolecules including proteinaceous remains were detected using more sensitive techniques, e.g. a combination of Tof-SIMS, Py-GC/MS, amino acid analysis, and in situ immunohistochemistry labeling (77).

Artificial thermal degradation experiments performed in various systems under well-constrained physical and chemical conditions have been carried out extensively to better understand thermal degradation process of keratins (42, 78–82). Our simulation experiments showed that feather material liquefies at temperature of 250°C (83). Previous thermal degradation studies revealed that the thermal decomposition of feathers begins at 220°C, and its maximum occurs at ~300°C (78). When the temperatures are below 250°C, thermal pressure hydrolysis caused rearrangement of hydrogen bonds in the keratin structure, as evidenced by the peaks from 2,000 to 1,700 cm^{-1}, mainly correspond to the C=O stretching vibration, which is sensitive to H-bonding after the formation of strong hydrogen bonds (42, 84).

When the temperatures are below the thermal decomposition threshold, the treated feather is still intact with all shafts and vane in place, then displays the cracks when dried, as seen in fossil feathers (83), indicating that they had gone through dehydration during diagenesis. A similar pattern was observed in another thermal degradation experiment on chicken feathers of different colors (82).

Similar lab simulations have been used a lot to better constrain the transformations of organic molecules into graphitic carbons induced by geochemical processes (e.g. (85, 86)). When the temperature is much higher and in dried conditions, pyrolysis of keratin will produce biocarbon (79), e.g. the FTIR spectra for the produced biocarbons at 600°C shows no peaks, which are a result of removing the functional groups at higher pyrolysis temperatures. A similar phenomenon has also been found in carbonized lignin (87). The FTIR spectra of all studied fossil feathers indicated that they were slightly matured, with a clear aliphatic absorption (at 1,375, 1,450, and 2,800–3,000 cm^{-1}) (85).

Preservation of melanin in fossils

Tof-SIMS has been successfully used to examine the melanin signals in fossils (77, 88, 89). In this work, Tof-SIMS showed peaks characteristic of eumelanin from all the Cretaceous feathers, and PCA analysis separated them from their associated sediments but closely located them around the eumelanin reference. Besides Tof-SIMS, Raman spectroscopy has also been widely used to detect eumelanin signals (26, 34, 90–92), which is characterized by two broad bands at ~1,360 and ~1,590 cm^{-1}. As previously noted, the disordered graphite of carbonaceous materials from geological sediments (27, 28) displayed the Raman spectra pattern with two similar bands. Peteya et al. (93) further compared the peaks generated by the fossil feather (containing melanosomes) to the *Platanus* (plant from the Late Cretaceous Hell Creek Formation, Mud Butters, North Dakota) and *Stigmaria* (from the Carboniferous Joggins Formation, Joggins, Nova Scotia) samples; the presented Raman spectra are similar to each other in both peak shape and location. In our work, when we compared the Raman spectra from fossil feathers with that from structureless organic remains in the sediments from the Yixian Formation (which was assumed to be experienced the same maturity), the peak location was similar, but the peak morphologies were different. PCA analysis can well separate the fossil feathers from the carbonaceous materials in sediments and humic acids.

Implications for the fossilization process of melanins in feathers

Melanins are the most prevalent pigments in animals, which is low solubility in distilled water and most organic and inorganic solvents, except for aqueous alkali. They are resistant to degradation by concentrated acids, and have a high resistance to thermal degradation (94). As previous discussed in the section on the fossilization process of keratins in feathers, we argued that the biodegradation process on fossil feathers was hindered, and the main degradation process was due to the long-term thermal degradation. Thus, the detected melanin from the fossil feathers should have also experienced a long-term thermal degradation. The thermal stability of melanins has been tested using thermogravimetric analysis (94). The results suggested three stages involved in the thermal degradation process: (i) evaporation of weakly and/or strongly bound water (around 60 – 280°C); (ii) the loss of carbon dioxide (around 306–425°C); (iii) the complete degradation (around 500–1,000°C). Compared to the keratins, melanin has a higher resistance to thermal degradation, which is confirmed in our simulation experiments. When the treated temperature reached 250°C, keratins were liquefied and melanosomes remained intact (83). The characteristic peaks of the keratins were almost diminished from the FTIR spectrum collected from the sample with the treated temperature reaching 250°C, but the Raman spectrum of the same sample retained the eumelanin signals.

Conclusion

The studied Cretaceous fossil feathers showed little evidence of keratin preservation based on FTIR. However, the same fossil feathers retained strong signals characteristic of melanins using ToF-SIMS and Raman spectroscopy. This differential preservation is attributed to the higher thermal stability of melanins compared with keratins. Experimental evidence and thermal degradation studies indicate that while keratins start degrading around 220–250°C, melanins can withstand much higher temperatures (up to 500–1,000°C) before complete degradation. Therefore, the fossil feathers, which experienced long-term thermal maturation during fossilization, preferentially preserved the more thermally stable melanin molecules over the less stable keratins. This selective preservation of biomolecules based on their thermal resistance allowed the retention of melanin biosignals in these low-maturity carbonaceous fossils.

Low-maturity carbonaceous fossils can indeed preserve biosignals, especially signals from molecules with high resistance to thermal degradation. As keratins are resistant to biodegradation due to their complex, rigid, and fibrous structure, they can still undergo degradation during the fossilization process, particularly through thermal maturation. The Oligocene TF feather is less thermally matured, giving it a higher potential to preserve keratin remains. However, distinguishing the FTIR signals of keratin remnants from microbial contamination is challenging. Therefore, further destructive analysis is essential. Alternatively, examining uncontaminated materials could provide clarity on this point (95–98).

Acknowledgments

We thank two reviewers for their helpful comments on our manuscript. We are grateful to P. Sjövall, J. Lindgren, Z.-H. Zhou, and M. Schweitzer for discussion and help in this study, and T. Zhao (Yunnan University) assisted during the data collection and analysis. X. Yang and B.-Y. Zhao (Guangzhou Institute of Geochemistry, Chinese Academy of Sciences) assisted during maturation experiments; Y.-X. Wang (Nanjing University) assisted during SEM observations and Raman analysis; L.-S. Zhang assisted during ATR-FTIR analysis; C.-S. Hu and H.-J. Liu (Infrared microspectroscopy and imaging beamline (BL 01B) of National Synchrotron Radiation Laboratory, University of Science and Technology of China) assisted during SR-FTIR-ATR analysis; and C. Guo, Q. Li, and Z.-P. Li (Tsinghua University) assisted during ToF-SIMS analysis.

Supplementary Material

Supplementary material is available at *PNAS Nexus* online.

Funding

The research was supported by the National Natural Science Foundation of China (grant numbers 42288201 and 41922011) and the Strategic Priority Research Program of Chinese Academy of Sciences (grant number XDB26000000), and the Fundamental Research Funds for the Central Universities (grant number 0206-14380219).

Author Contributions

Y.P.: conceptualization, data curation, formal analysis, investigation, visualization, writing—original draft, writing—review and editing. Z.Q.: data curation, investigation, methodology, writing—review and editing. J.H.: formal analysis, investigation, methodology, writing—review and editing. X.Z.: resources, investigation, writing—review and editing. X.W.: resources, investigation, writing—review and editing.

Data Availability

Data generated in this study are shared in Supplementary Datasets S1, S4–S6. Tof-SIMS analysis results data (Figs. S2 and S3) have been deposited in Science Data Bank (https://www.scidb.cn/en/anonymous/aUFGZkly). All other data are included in the manuscript and/or supporting information.

References

1 Benton MJ, Dhouailly D, Jiang B, McNamara M. 2019. The early origin of feathers. *Trends Ecol Evol*. 34:856–869.
2 Li Q, *et al.* 2014. Melanosome evolution indicates a key physiological shift within feathered dinosaurs. *Nature*. 507:350–353.
3 Xu X, *et al.* 2014. An integrative approach to understanding bird origins. *Science*. 346:1253293.
4 Colleary C, *et al.* 2015. Chemical, experimental, and morphological evidence for diagenetically altered melanin in exceptionally preserved fossils. *Proc Natl Acad Sci U S A*. 112:12592–12597.
5 Lindgren J, *et al.* 2015. Molecular composition and ultrastructure of jurassic paravian feathers. *Sci Rep*. 5:13520.
6 Pan Y, *et al.* 2016. Molecular evidence of keratin and melanosomes in feathers of the Early Cretaceous bird *Eoconfuciusornis*. *Proc Natl Acad Sci U S A*. 113:E7900–E7907.
7 Pan Y, *et al.* 2019. The molecular evolution of feathers with direct evidence from fossils. *Proc Natl Acad Sci U S A*. 116:3018–3023.
8 Schweitzer MH, *et al.* 1999. Beta-keratin specific immunological reactivity in feather-like structures of the Cretaceous Alvarezsaurid, *Shuvuuia deserti*. *J Exp Zool*. 285:146–157.
9 Alibardi L. 2017. Review: cornification, morphogenesis and evolution of feathers. *Protoplasma*. 254:1259–1281.
10 Laurent CM, Dyke JM, Cook RB, Dyke G, de Kat R. 2020. Spectroscopy on the wing: investigating possible differences in protein secondary structures in feather shafts of birds using Raman spectroscopy. *J Struct Biol*. 211:107529.
11 Weiss IM, Kirchner HOK. 2011. Plasticity of two structural proteins: alpha-collagen and beta-keratin. *J Mech Behav Biomed Mater*. 4:733–743.
12 Saitta ET, *et al.* 2018. Preservation of feather fibers from the late cretaceous dinosaur *Shuvuuia deserti* raises concern about immunohistochemical analyses on fossils. *Org Geochem*. 125:142–151.
13 Saitta ET, *et al.* 2017. Low fossilization potential of keratin protein revealed by experimental taphonomy. *Palaeontology*. 60:547–556.
14 Saitta ET, Vinther J. 2019. A perspective on the evidence for keratin protein preservation in fossils: an issue of replication versus validation. *Palaeontologia Electronica*. 22.3.2E:1–30.
15 D'Alba L, Shawkey MD. 2019. Melanosomes: biogenesis, properties, and evolution of an ancient organelle. *Physiol Rev*. 99:1–19.
16 Manning PL, *et al.* 2019. Pheomelanin pigment remnants mapped in fossils of an extinct mammal. *Nat Commun*. 10:2250.
17 Hu D, *et al.* 2018. A bony-crested jurassic dinosaur with evidence of iridescent plumage highlights complexity in early paravian evolution. *Nat Commun*. 9:217.
18 Li Q, *et al.* 2012. Reconstruction of *Microraptor* and the evolution of iridescent plumage. *Science*. 335:1215–1219.
19 Li Q, *et al.* 2010. Plumage color patterns of an extinct dinosaur. *Science*. 327:1369–1372.
20 Zhang F, *et al.* 2010. Fossilized melanosomes and the colour of Cretaceous dinosaurs and birds. *Nature*. 463:1075–1078.
21 Lhoest J-B, Wagner MS, Tidwell CD, Castner DG. 2001. Characterization of adsorbed protein films by time of flight secondary ion mass spectrometry. *J Biomed Mater Res*. 57:432–440.
22 Sanni OD, Wagner MS, Briggs D, Castner DG, Vickerman JC. 2002. Classification of adsorbed protein static ToF-SIMS spectra by principal component analysis and neural networks. *Surf Interface Anal*. 33:715–728.
23 Wagner MS, Castner DG. 2001. Characterization of adsorbed protein films by time-of-flight secondary ion mass spectrometry with principal component analysis. *Langmuir*. 17:4649–4660.
24 Roldán ML, Centeno SA, Rizzo A. 2014. An improved methodology for the characterization and identification of sepia in works of art by normal Raman and SERS, complemented by FTIR, py-GC/MS, and XRF. *J Raman Spectrosc*. 45:1160–1171.
25 Gunasekaran S, Anbalagan G, Pandi S. 2006. Raman and infrared spectra of carbonates of calcite structure. *J Raman Spectrosc*. 37:892–899.
26 Galván I, Jorge A. 2015. Dispersive Raman spectroscopy allows the identification and quantification of melanin types. *Ecol Evol*. 5:1425–1431.
27 Kouketsu Y, *et al.* 2014. A new approach to develop the Raman carbonaceous material geothermometer for low-grade metamorphism using peak width. *Island Arc*. 23:33–50.
28 Rahl JM, Anderson KM, Brandon MT, Fassoulas C. 2005. Raman spectroscopic carbonaceous material thermometry of low-grade metamorphic rocks: calibration and application to tectonic exhumation in Crete, Greece. *Earth Planet Sci Lett*. 240:339–354.
29 Perna G, Lasalvia M, Capozzi V. 2016. Vibrational spectroscopy of synthetic and natural eumelanin. *Polym Int*. 65:1323–1330.
30 Bada JL, Wang XS, Hamilton H. 1999. Preservation of key biomolecules in the fossil record: current knowledge and future challenges. *Philos Trans R Soc Lond B Biol Sci*. 354:77–87.
31 Manning PL, *et al.* 2009. Mineralized soft-tissue structure and chemistry in a mummified hadrosaur from the hell creek formation, North Dakota (USA). *Proc R Soc Lond B Biol Sci*. 276:3429–3437.
32 Glass KE. 2014. *Chemical and physical analysis of melanin in complex biological matrices*. Durham: Duke University.
33 Pan Y, Hu L, Zhao T. 2019. Applications of chemical imaging techniques in paleontology. *Natl Sci Rev*. 6:1040–1053.
34 Centeno SA, Shamir J. 2008. Surface enhanced Raman scattering (SERS) and FTIR characterization of the sepia melanin pigment used in works of art. *J Mol Struct*. 873:149–159.
35 Machado W, Franchini JC, de Fátima Guimarães M, Filho JT. 2020. Spectroscopic characterization of humic and fulvic acids in soil aggregates, Brazil. *Heliyon*. 6:e04078.
36 Barden HE, *et al.* 2011. Morphological and geochemical evidence of eumelanin preservation in the feathers of the Early Cretaceous bird, *Gansus yumenensis*. *PLoS One*. 6:e25494.
37 Cincotta A, *et al.* 2020. Chemical preservation of tail feathers from *Anchiornis huxleyi*, a theropod dinosaur from the Tiaojishan formation (Upper Jurassic, China). *Palaeontology*. 63:841–863.
38 Edwards NP, *et al.* 2011. Infrared mapping resolves soft tissue preservation in 50 million year-old reptile skin. *Proc R Soc Lond B Biol Sci*. 278:3209–3218.
39 Yang Z, *et al.* 2019. Pterosaur integumentary structures with complex feather-like branching. *Nat Ecol Evol*. 3:24–30.

40 Brandelli A. 2008. Bacterial keratinases: useful enzymes for bioprocessing agroindustrial wastes and beyond. *Food Bioprocess Technol*. 1:105–116.

41 Greenwold MJ, *et al*. 2014. Dynamic evolution of the alpha (α) and beta (β) keratins has accompanied integument diversification and the adaptation of birds into novel lifestyles. *BMC Evol Biol*. 14:249.

42 Windt X, *et al*. 2022. Fourier transform infrared spectroscopy for assessing structural and enzymatic reactivity changes induced during feather hydrolysis. *ACS Omega*. 7:39924–39930.

43 Salminen E, Rintala J. 2002. Anaerobic digestion of organic solid poultry slaughterhouse waste–a review. *Bioresour Technol*. 83: 13–26.

44 Vidmar B, Vodovnik M. 2018. Microbial keratinases: enzymes with promising biotechnological applications. *Food Technol Biotechnol*. 56:312–328.

45 Błyskal B. 2009. Fungi utilizing keratinous substrates. *Int Biodeterior Biodegrad*. 63:631–653.

46 Gupta R, Ramnani P. 2006. Microbial keratinases and their prospective applications: an overview. *Appl Microbiol Biotechnol*. 70: 21–33.

47 Solazzo C, *et al*. 2013. Proteomic evaluation of the biodegradation of wool fabrics in experimental burials. *Int Biodeterior Biodegrad*. 80:48–59.

48 Grumbt M, *et al*. 2013. Keratin degradation by dermatophytes relies on cysteine dioxygenase and a sulfite efflux pump. *J Invest Dermatol*. 133:1550–1555.

49 Lange L, Huang Y, Busk PK. 2016. Microbial decomposition of keratin in nature—a new hypothesis of industrial relevance. *Appl Microbiol Biotechnol*. 100:2083–2096.

50 Yamamura S, Morita Y, Hasan Q, Yokoyama K, Tamiya E. 2002. Keratin degradation: a cooperative action of two enzymes from *Stenotrophomonas* sp. *Biochem Biophys Res Commun*. 294:1138–1143.

51 Ramnani P, Singh R, Gupta R. 2005. Keratinolytic potential of *Bacillus licheniformis* RG1: structural and biochemical mechanism of feather degradation. *Can J Microbiol*. 51:191–196.

52 Vignardet C, Guillaume Y, Michel L, Friedrich J, Millet J. 2001. Comparison of two hard keratinous substrates submitted to the action of a keratinase using an experimental design. *Int J Pharm*. 224:115–122.

53 Gupta S, Singh R. 2014. Hydrolyzing proficiency of keratinases in feather degradation. *Indian J Microbiol*. 54:466–470.

54 He Z, *et al*. 2018. Biodegradation of feather waste keratin by the keratin-degrading strain Bacillus subtilis 8. *J Microbiol Biotechnol*. 28:314–322.

55 Lai Y, Wu X, Zheng X, Li W, Wang L. 2023. Insights into the keratin efficient degradation mechanism mediated by *Bacillus* sp. CN2 based on integrating functional degradomics. *Biotechnol Biofuels Bioprod*. 16:59.

56 Nnolim NE, Okoh AI, Nwodo UU. 2020. *Bacillus* sp. FPF-1 produced keratinase with high potential for chicken feather degradation. *Molecules*. 25:1505.

57 Sharma C, Timorshina S, Osmolovskiy A, Misri J, Singh R. 2022. Chicken feather waste valorization into nutritive protein hydrolysate: role of novel thermostable keratinase from *Bacillus pacificus* RSA27. *Front Microbiol*. 13:882902.

58 Gessesse A, Hatti-Kaul R, Gashe BA, Mattiasson B. 2003. Novel alkaline proteases from alkaliphilic bacteria grown on chicken feather. *Enzyme Microb Technol*. 32:519–524.

59 Manczinger L, Rozs M, Vágvölgyi C, Kevei F. 2003. Isolation and characterization of a new keratinolytic *Bacillus licheniformis* strain. *World J Microbiol Biotechnol*. 19:35–39.

60 Daroit DJ, Brandelli A. 2014. A current assessment on the production of bacterial keratinases. *Crit Rev Biotechnol*. 34:372–384.

61 Sonenshein AL. 2005. Cody, a global regulator of stationary phase and virulence in Gram-positive bacteria. *Curr Opin Microbiol*. 8: 203–207.

62 Fürsich FT, Sha J, Jiang B, Pan Y. 2007. High resolution palaeoecological and taphonomic analysis of Early Cretaceous lake biota, western Liaoning (NE-China). *Palaeogeogr Palaeoclimatol Palaeoecol*. 253:434–457.

63 Pan Y, *et al*. 2012. Dynamics of the lacustrine fauna from the Early Cretaceous yixian formation, China: implications of volcanic and climatic factors. *Lethaia*. 45:299–314.

64 Abdel-Fattah AM, El-Gamal MS, Ismail SA, Emran MA, Hashem AM. 2018. Biodegradation of feather waste by keratinase produced from newly isolated *Bacillus licheniformis* ALW1. *J Genet Eng Biotechnol*. 16:311–318.

65 Barman NC, *et al*. 2017. Production, partial optimization and characterization of keratinase enzyme by *Arthrobacter* sp. NFH5 isolated from soil samples. *AMB Express*. 7:181.

66 Chaisemsaeng P, Ansanan S, Sirisan S. 2017. Feather degradation and keratinase production by *Bacillus* sp. and *Lactobacillus* sp. *Int J Biotech Res*. 7:29–36.

67 Han M, Luo W, Gu Q, Yu X. 2012. Isolation and characterization of a keratinolytic protease from a feather-degrading bacterium *Pseudomonas aeruginosa* C11. *Afr J Microbiol Res*. 6(9):2211–2221.

68 Ire F, Onyenama A. 2017. Effects of some cultural conditions on keratinase production by *Bacillus licheniformis* strain NBRC 14206. *J Adv Biol Biotechnol*. 13:1–13.

69 Mazotto AM, *et al*. 2011. Biodegradation of feather waste byextracellular keratinases and gelatinases from *Bacillus* spp. *World J Microbiol Biotechnol*. 27:1355–1365.

70 Okoroma EA, Garelick H, Abiola OO, Purchase D. 2012. Identification and characterisation of a *Bacillus licheniformis* strain with profound keratinase activity for degradation of melanised feather. *Int Biodeterior Biodegrad*. 74:54–60.

71 Zhang R, *et al*. 2022. Production of surfactant-stable keratinase from *Bacillus cereus* YQ 15 and its application as detergent additive. *BMC Biotechnol*. 22:26.

72 Fürsich FT, Pan Y-H, Wang Y-Q. 2016. Biostratinomy of bivalves from jurassic and Early Cretaceous lakes of NE China. *Palaeoworld*. 25:399–405.

73 Pan Y, Sha J, Yao X. 2012. Taphonomy of Early Cretaceous freshwater bivalve concentrations from the Sihetun area, western Liaoning, NE China. *Cretac Res*. 34:94–106.

74 Hu L, Zhao T, Pan Y. 2020. Spinicaudatans from the Yixian formation (lower Cretaceous) and the daohugou beds (Jurassic) of Western Liaoning, China. *Cretac Res*. 105:104073.

75 Pan Y, Wang Y, Sha J, Liao H. 2015. Exceptional preservation of clam shrimp (Branchiopoda, Eucrustacea) eggs from the Early Cretaceous jehol biota and implications for paleoecology and taphonomy. *J Paleontol*. 89:369–376.

76 Bobroff V, Chen H-H, Javerzat S, Petibois C. 2016. What can infrared spectroscopy do for characterizing organic remnant in fossils? *Trends Analyt Chem*. 82:443–456.

77 Lindgren J, *et al*. 2018. Soft-tissue evidence for homeothermy and crypsis in a jurassic ichthyosaur. *Nature*. 564:359–365.

78 Kluska J, Kardaś D, Heda Ł, Szumowski M, Szuszkiewicz J. 2016. Thermal and chemical effects of Turkey feathers pyrolysis. *Waste Manag*. 49:411–419.

79 Li Z, Reimer C, Picard M, Mohanty AK, Misra M. 2020. Characterization of chicken feather biocarbon for use in sustainable biocomposites. *Front Mater*. 7:3.

80 Munagala CK, *et al.* 2022. Chicken feather thermal decomposition analysis and techno-economic assessment for production of value-added products: a pilot plant study. *Biomass Convers Biorefin*. 1–24.
81 Senoz E, Wool RP. 2010. Microporous carbon–nitrogen fibers from keratin fibers by pyrolysis. *J Appl Polym Sci*. 118:1752–1765.
82 Tuna A, Okumuş Y, Celebi H, Seyhan AT. 2015. Thermochemical conversion of poultry chicken feather fibers of different colors into microporous fibers. *J Anal Appl Pyrolysis*. 115:112–124.
83 Zhao T, Hu J, Hu L, Pan Y. 2020. Experimental maturation of feathers: implications for interpretations of fossil feathers. *PALAIOS*. 35:67–76.
84 Brebu M, Spiridon I. 2011. Thermal degradation of keratin waste. *J Anal Appl Pyrolysis*. 91:288–295.
85 Lis GP, Mastalerz M, Schimmelmann A, Lewan MD, Stankiewicz BA. 2005. FTIR absorption indices for thermal maturity in comparison with vitrinite reflectance R0 in type-II kerogens from Devonian black shales. *Org Geochem*. 36:1533–1552.
86 Vandenbroucke M, Largeau C. 2007. Kerogen origin, evolution and structure. *Org Geochem*. 38:719–833.
87 Snowdon MR, Mohanty AK, Misra M. 2014. A study of carbonized lignin as an alternative to carbon black. *ACS Sustain Chem Eng*. 2: 1257–1263.
88 Lindgren J, *et al.* 2019. Fossil insect eyes shed light on trilobite optics and the arthropod pigment screen. *Nature*. 573:122–125.
89 Lindgren J, *et al.* 2014. Skin pigmentation provides evidence of convergent melanism in extinct marine reptiles. *Nature*. 506:484–488.
90 Galván I, *et al.* 2013. Raman spectroscopy as a non-invasive technique for the quantification of melanins in feathers and hairs. *Pigment Cell Melanoma Res*. 26:917–923.
91 Huang Z, *et al.* 2004. Raman spectroscopy of *in vivo* cutaneous melanin. *J Biomed Opt*. 9:1198–1205.
92 Perna G, Lasalvia M, Gallo C, Quartucci G, Capozzi V. 2013. Vibrational characterization of synthetic eumelanin by means of Raman and surface enhanced Raman scattering. *Open Surf Sci J*. 5:1–8.
93 Peteya JA, Clarke JA, Li Q, Gao K-Q, Shawkey MD. 2017. The plumage and colouration of an enantiornithine bird from the Early Cretaceous of China. *Palaeontology*. 60:55–71.
94 Pralea I-E, *et al.* 2019. From extraction to advanced analytical methods: the challenges of melanin analysis. *Int J Mol Sci*. 20: 3943.
95 Henry DG, Jarvis I, Gillmore G, Stephenson M, Emmings JF. 2018. Assessing low-maturity organic matter in shales using Raman spectroscopy: effects of sample preparation and operating procedure. *Int J Coal Geol*. 191:135–151.
96 Hu C, Wang X, Qi Z, Li C. 2020. The new infrared beamline at NSRL. *Infrared Phys Technol*. 105:103200.
97 Lee JLS, Gilmore IS, Seah MP. 2008. Proposed terminology for multivariate analysis in surface chemical analysis–vocabulary–part 1: general terms and terms for the spectroscopies. *Chem Anal*. 1–10.
98 Stevens A, Ramirez-Lopez L. 2021. An introduction to the "prospectr" package.